

Bioinspired Hydrogel with Tailored Nano-topography and Desired Mechanical Performance for Highly Efficient Solar-Driven Water Purification

Wenjing Ma, Wenxuan Cao, Min Cui, Qinwei Fan, Ranhua Xiong, Chaobo Huang*

Joint Laboratory of Advanced Biomedical Materials (NFU-UGent), Jiangsu Co-Innovation Center of Efficient Processing and Utilization of Forest Resources, Nanjing Forestry University, Nanjing 210037, P. R. China

Corresponding authors: Chaobo.Huang@njfu.edu.cn (Chaobo Huang)



Figure S1 Photograph of the hydrogel with “NJFU” shapes.

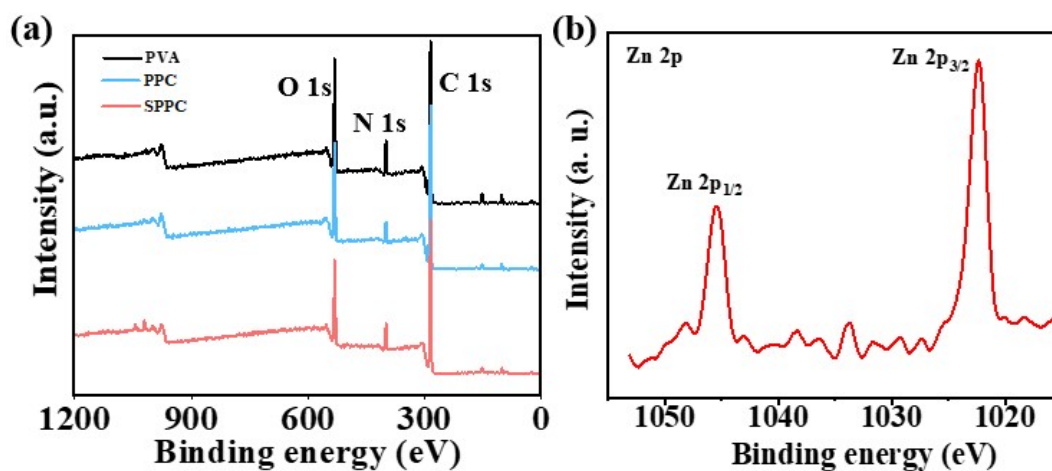


Figure S2 (a) XPS spectra of different hydrogels samples: (b) XPS spectra of Zn 2p of SPPC hydrogel.

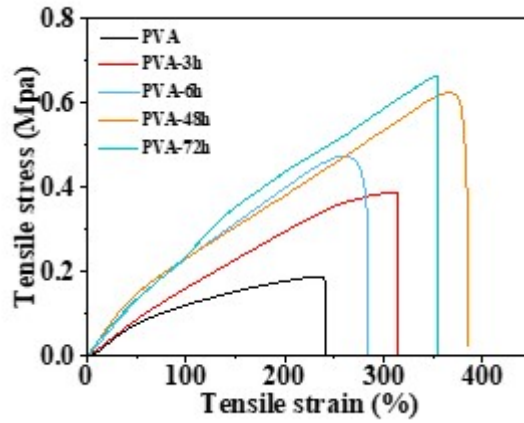


Figure S3 Mechanical properties of hydrogels with different soaking time.

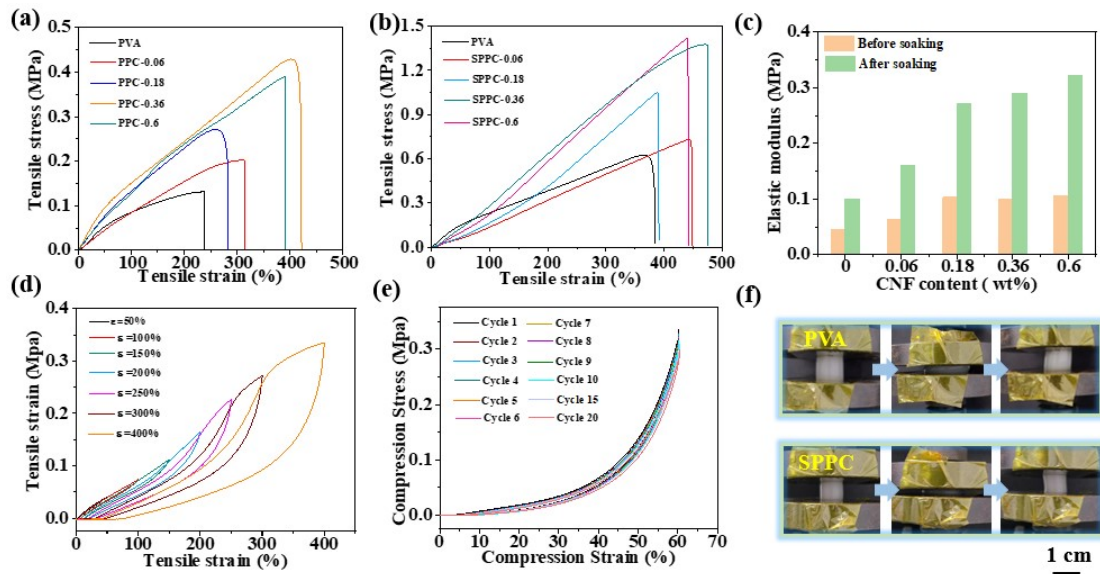


Figure S4 Stress–strain curves of (a) PPC and SPPC (b) hydrogels with different CNF contents. (c) Elastic modulus of the SPPC hydrogel with various CNF content. (d) Successive tensile loading–unloading stress–strain curves of the PPC hydrogel. (e) The results of a 100-cycle fatigue test on the PPC hydrogel at a compressive strain of 70%. (f) The compression process of PVA and PPC hydrogels.

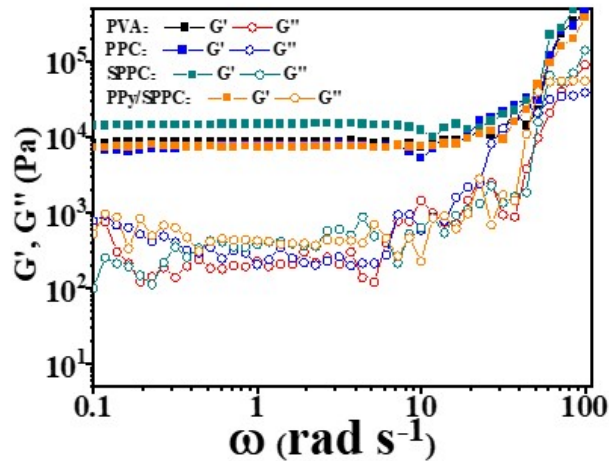


Figure S5 Angular frequency sweeping measurements of different hydrogels at a constant strain of 0.5%.

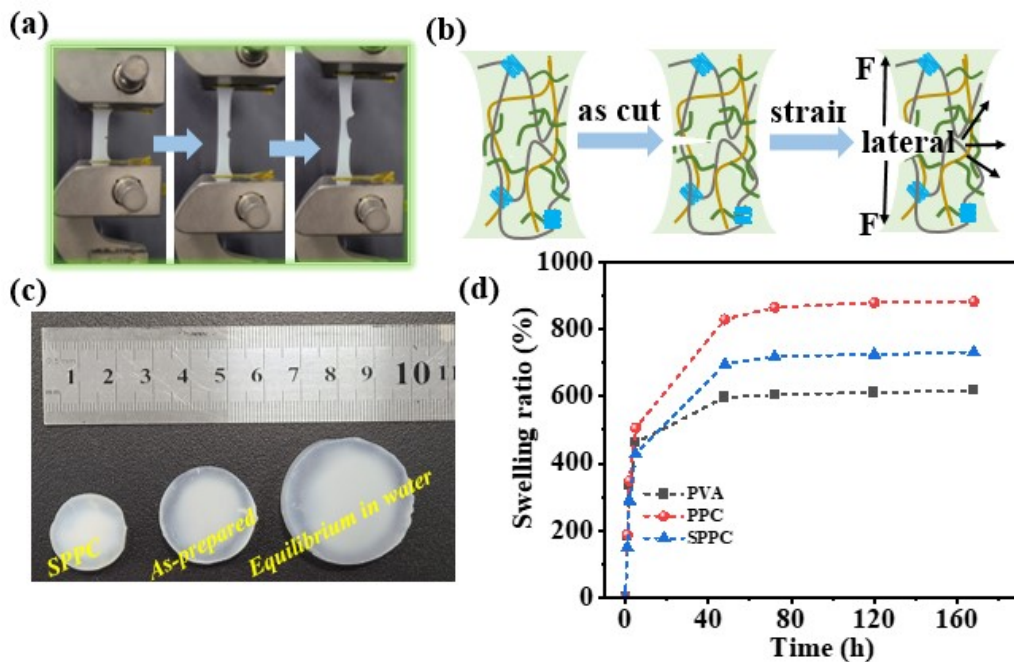


Figure S6 (a) Photographs showing the crack resistance of the PPC hydrogel at the strain of 200%. (b) Schematic diagrams of notch expansion during stretching of the PPC hydrogel. (c) Optical micrograph of the PPC hydrogel equilibrated in water states. (d) Volume swelling ratio and average pore diameter of the tested hydrogels.

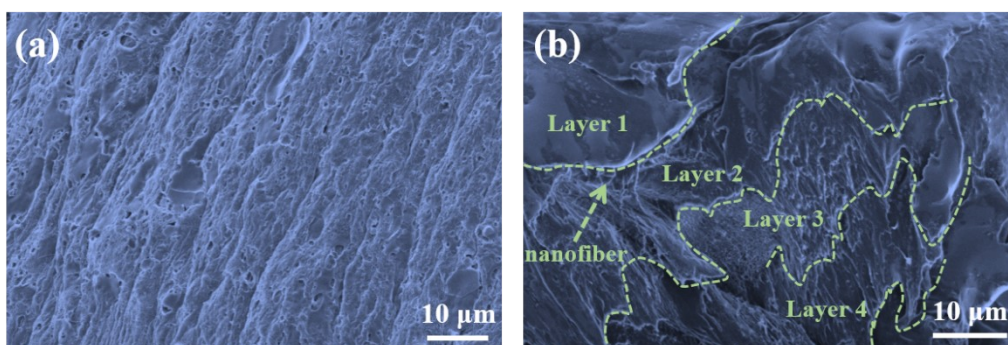


Figure S7 SEM image of (a) PPC and (b) SPPC hydrogels tensile fracture surface.

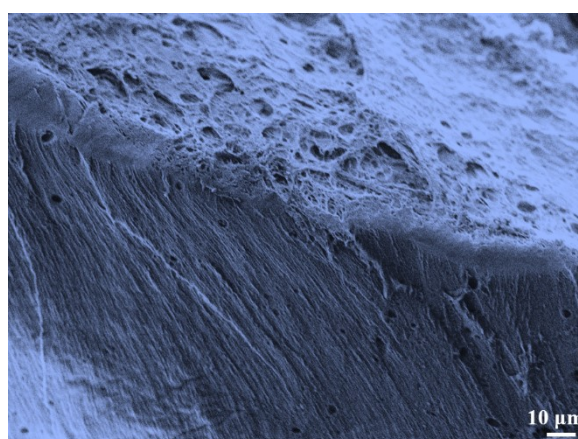


Figure S8 SEM image of the interface between PPy and hydrogel.

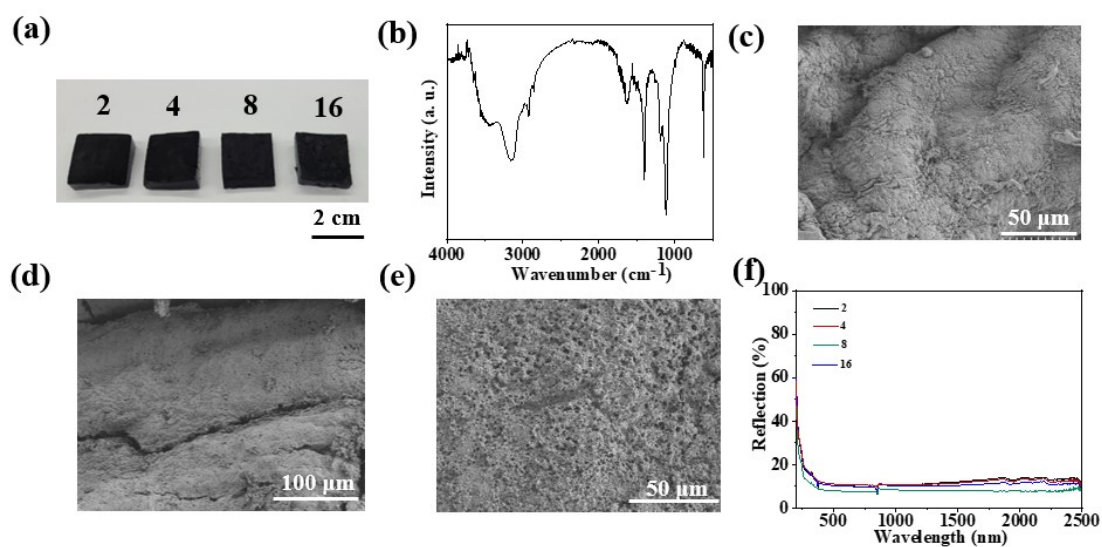


Figure S9 (a) Photographs of PPy/SPPC hydrogel with different numbers of PPy layers. (b) The FTIR spectrum of PPy/SPPC hydrogel. Top-view SEM images of PPy/SPPC hydrogel with different numbers of PPy layers. (c) 2, (d) 4, (e) 16, (f) Diffuse reflectance spectra of the PPy/SPPC hydrogel with different layers of PPy nanosheets.

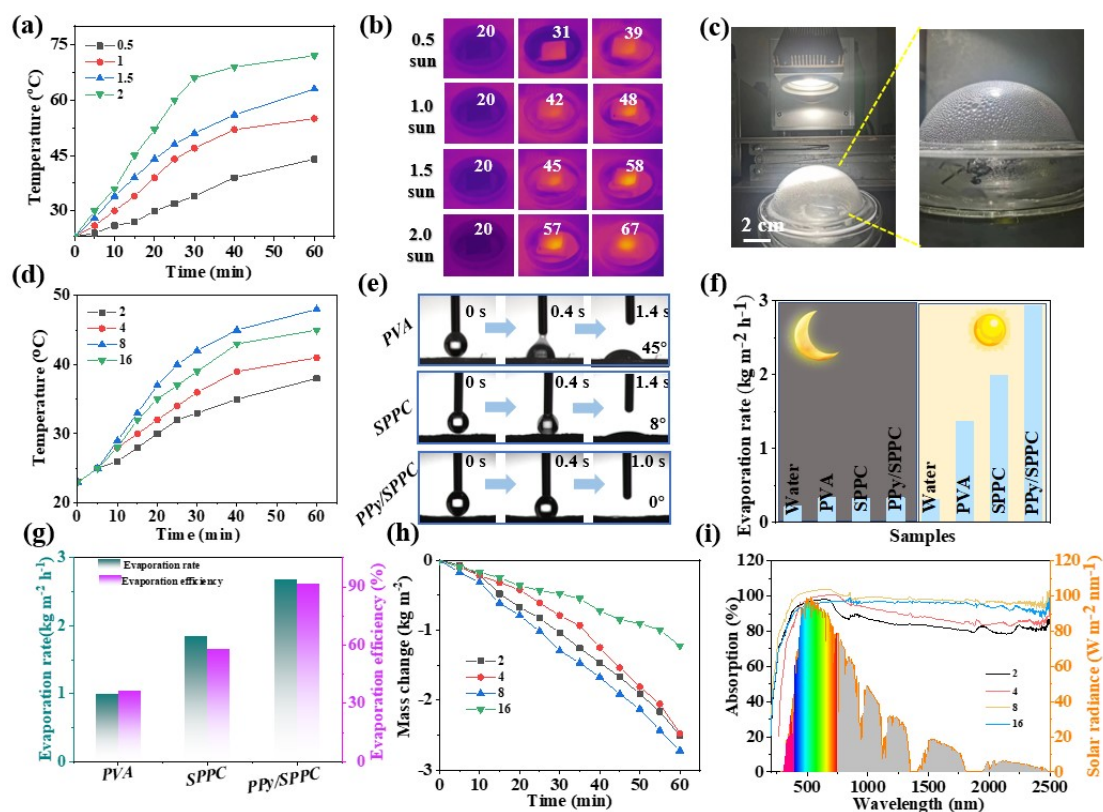


Figure S10 (a) The surface temperature change of PPy/SPPC under different light intensity. (b) The IR images of PPy/SPPC under different rate solar illumination. (c) The actual photo of PPy/SPPC in the process of solar evaporation. (d) The surface temperature change of the PPy/SPPC hydrogel with different layers of PPy nanosheets. (e) Water contact angle measurements of different hydrogels. (f) Water evaporation rates in dark and light conditions. (g) Evaporation rates and efficiency of teste hydrogels. (h) Mass changes versus time of PPy/SPPC with different layers of PPy nanosheets. (i) Transmittance reflectance spectra of PPy/SPPC with different layers of PPy nanosheets.

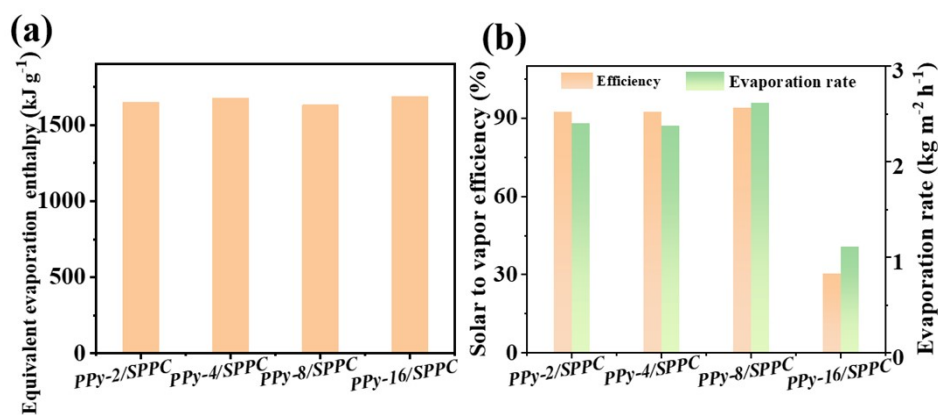


Figure S11 (a) The equivalent evaporation enthalpy and evaporation rate, solar to vapor efficiency of the PPy/SPPC hydrogel with different layers of PPy nanosheets (b).

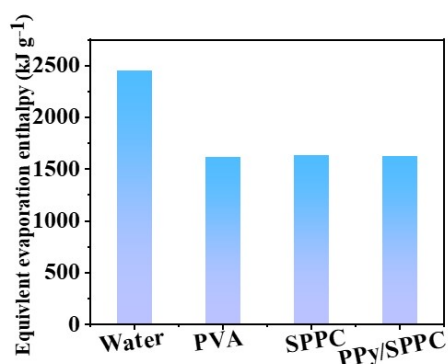


Figure S12 The equivalent evaporation enthalpy of the different hydrogels.

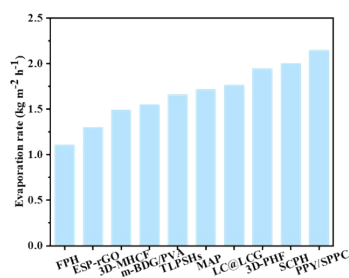


Figure S13 Evaporation rates of different evaporators in simulated seawater (3.5wt % NaCl solution)¹⁻⁹.

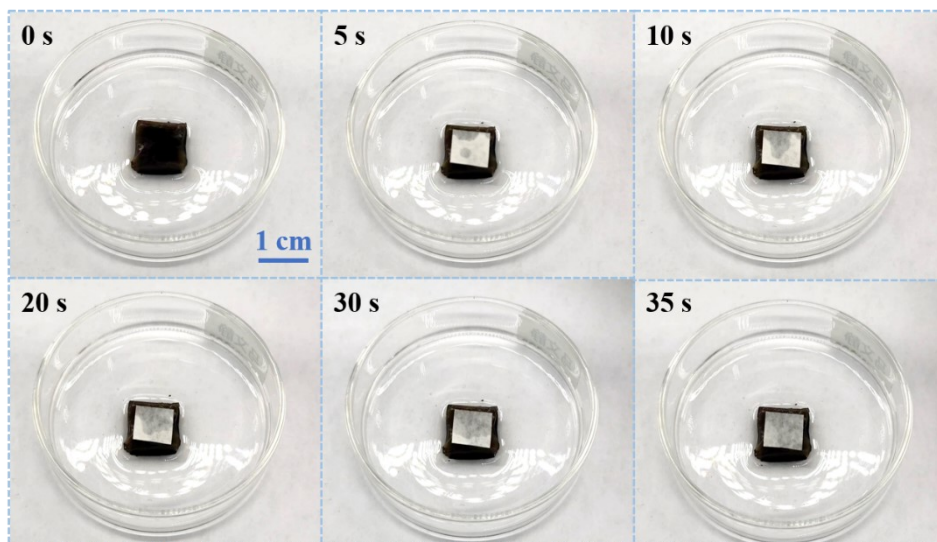


Figure S14 The transfer process of water on PPy/SPPC.

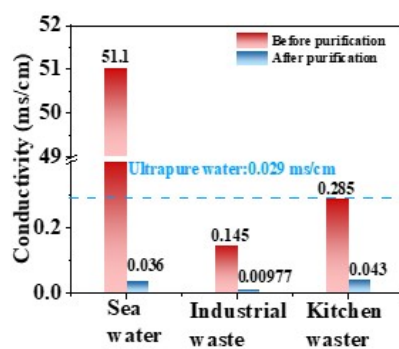


Figure S15 Conductivity of Seawater, industrial wastewater and kitchen wastewater before and after purification.

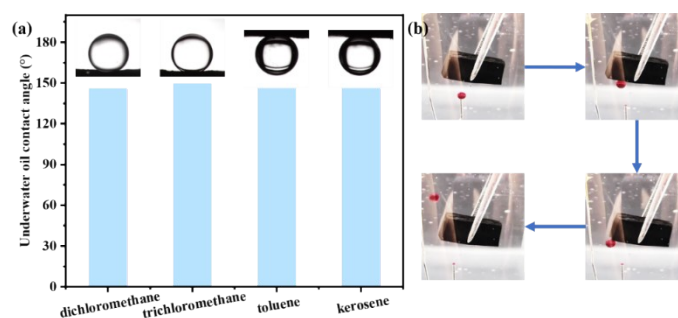


Figure S16 (a) Underwater oil contact angle measurements of PPy/SPPC. (b) Underwater antifouling of PPy/SPPC evaporator.

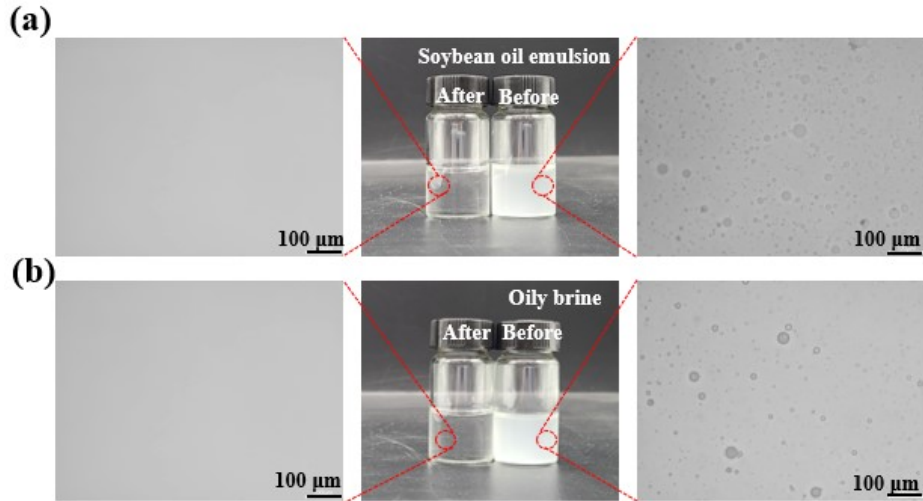


Figure S17 Optical and the corresponding microscopic pictures of the (a) soybean oil emulsion and oily brine (b) before and after purification.

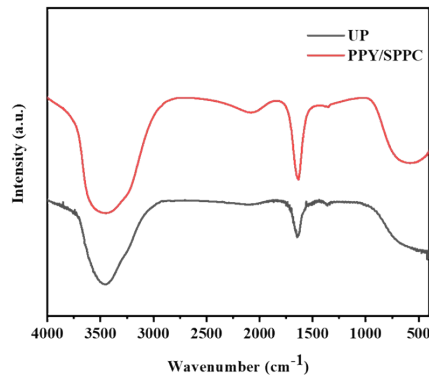


Figure S18 FTIR spectra of ultra-pure water and PPY/SPPC leach solution.

Calculations of the Heat Loss

The heat loss during the evaporation process is mainly caused by three aspects, including radiation, convection and conduction. The detailed calculation methods are as follows:

1) Radiation Loss

The radiation loss can be calculated by Stefan-Boltzmann:

$$\Phi = \varepsilon A \sigma (T_1^4 - T_2^4) \quad (S1)$$

where Φ represents the heat flux, ε is the denotes emissivity (Supposing the evaporator has a maximum emissivity of 1), A is the evaporation surface area (0.0007 m^2), σ is the

Stefan-Boltzmann constant ($5.67 \times 10^{-8} \text{ W m}^{-2} \cdot \text{K}^{-4}$), T_1 is the average surface temperature of the evaporator (48 °C for SPPC, 32.5 °C for PPC, 33 °C PVA), and T_2 is the ambient temperature (20 °C). Therefore, based on Eq. S1, we can calculate that the radiation loss of PPy/SPPC, SPPC, PVA accounts for ~12.9%, 5.3%, 5.5%, respectively (under 1-sun illumination).

2) Convection Loss

The heat convection occurs between the solar absorber surface and the ambient environment. Then, the radiation loss can be calculated by Newton's law.

$$Q = hA(T_1 - T_2) \quad (\text{S2})$$

where Q denotes the heat, h is the convection heat transfer coefficient (according to an early report, the convection heat transfer coefficient is about $5 \text{ W m}^{-2} \text{ K}^{-1}$), A is the surface area of the absorber (0.0007 m^2), T_1 is the average surface temperature of the absorber, and T_2 is the ambient temperature.

Therefore, based on Eq. S2, we can calculate that the radiation loss of PPy/SPPC, SPPC, PVA accounts for ~9.8%, 4.3%, 4.5%, respectively. (under 1-sun illumination) of all the irradiation energy.

3) Conduction Loss

Here, the conduction loss refers to the heat from absorber to bulk water. In order to calculate the conduction loss, the entire vaporization system was put in a Dewar container under 1-sun illumination. Then, the conduction loss can be calculated by the following equation:

$$Q = Cm\Delta T \quad (\text{S3})$$

where Q denotes the heat, C is the specific heat capacity of water ($4.2 \text{ J g}^{-1} \text{ K}^{-1}$), m is the water weight (25 g), and ΔT is the elevated water temperature within 3600 s (1.1 °C under 1-sun illumination).

Therefore, based on Eq. S3, we can calculate that the radiation loss accounts for ~1.74% (under 1-sun illumination) of all the irradiation energy. (Note: As the evaporation experiment proceeds the water weight is constantly decreasing. Therefore,

the calculated radiation loss value is larger than the actual value.)

Table S1. Recipes of hydrogels

Hydrogels	H ₂ O (mL)	CNF content (wt%)	APS (g)	TEMED (μ L)
PVA	5	0	0.025	100
PPC-0.06	5	0.06	0.025	100
PPC-0.18	5	0.18	0.025	100
PPC-0.36	5	0.36	0.025	100
PPC-0.6	5	0.6	0.025	100

References

1. X. Liang, X. Zhang, Q. Huang, H. Zhang, C. Liu and Y. Liu, *Solar Energy*, 2020, **208**, 778-786.
2. Y. Chen, H. Qiu, X. Li, Q. Tong, M. Jensen, Q. Li and N. Wang, *Applied Surface Science*, 2022, **582**.
3. L. Li, N. He, S. Yang, Q. Zhang, H. Zhang, B. Wang, T. Dong, H. Wang, B. Jiang and D. Tang, *EcoMat*, 2022, **5**.
4. X. Lin, P. Wang, R. Hong, X. Zhu, Y. Liu, X. Pan, X. Qiu and Y. Qin, *Advanced Functional Materials*, 2022, **32**.
5. B. Zhang, P. W. Wong and A. K. An, *Chemical Engineering Journal*, 2022, **430**.
6. D. Deng, Q. Liang, Z. Xiao and C. Liu, *Chemical Engineering Journal*, 2023, **474**.
7. L. Han, H. Zhou, M. Fu, J. Li, H. Ma and B. Zhang, *Chemical Engineering Journal*, 2023, **473**.
8. H. Zhou, L. Han, M. Yang, X. Wu, J. Li, H. Ma and B. Zhang, *Desalination*, 2023, **556**.
9. L. Han, M. Yang, H. Zhou, C. Hong, J. Li, H. Ma and B. Zhang, *Applied Surface Science*, 2024, **662**.